Bias Dependence of the Electrical Spin Injection into GaAs from Co – Fe – B / MgO Injectors with Different MgO Growth Processes

Philippe Barate, S. h. H Liang, Tiantian Zhang, J. Frougier, B. Xu, Philippe Schieffer, M. Vidal, H. Jaffres, B. Lépine, Sylvain Tricot, et al.

Bias Dependence of the Electrical Spin Injection into GaAs from Co-Fe-B/MgO Injectors with Different MgO Growth Processes

P. Barate,[1] S. H. Liang,[2,6] T. T. Zhang,[1] J. Frougier,[3] B. Xu,[4] P. Schieffer,[5] M. Vidal,[1] H. Jaffrès,[3] B. Lépine,[5] S. Tricot,[5] F. Cadiz,[1] T. Garandel,[1] J. M. George,[3] T. Amand,[1] X. Devaux,[2] M. Hehn,[2] S. Mangin,[2] B. Tao,[6] X. F. Han,[6] Z. G. Wang,[4] X. Marie,[1] Y. Lu,[2,*] and P. Renucci[1,†]

[1]*Université de Toulouse, INSA-CNRS-UPS, LPCNO, 135 Avenue de Rangueil, 31077 Toulouse, France*
[2]*Institut Jean Lamour, UMR 7198, CNRS—Université de Lorraine, B.P. 239, 54506 Vandoeuvre, France*
[3]*Unité Mixte de Physique CNRS/Thales and Université Paris–Sud 11, 1 Avenue Augustin Fresnel, 91767 Palaiseau, France*
[4]*Key Laboratory of Semiconductor Materials Science, Institute of Semiconductors, Chinese Academy of Sciences, P.O. Box 912, Beijing 100083, China*
[5]*Département Matériaux et Nanosciences, Institut de Physique de Rennes, UMR 6251, CNRS—Université de Rennes 1, Campus de Beaulieu, Bat 11 E, 35042 Rennes Cedex, France*
[6]*Beijing National Laboratory of Condensed Matter Physics, Institute of Physics, Chinese Academy of Sciences, Beijing 100190, China*

(Received 24 April 2017; revised manuscript received 7 July 2017; published 13 November 2017)

We investigate the influence of the MgO growth process on the bias dependence of the electrical spin injection from a Co-Fe-B/MgO spin injector into a GaAs-based light-emitting diode (spin LED). With this aim, textured MgO tunnel barriers are fabricated either by sputtering or molecular-beam-epitaxy (MBE) methods. For the given growth parameters used for the two techniques, we observe that the circular polarization of the electroluminescence emitted by spin LEDs is rather stable as a function of the injected current or applied bias for the samples with sputtered tunnel barriers, whereas the corresponding circular polarization decreases abruptly for tunnel barriers grown by MBE. We attribute these different behaviors to the different kinetic energies of the injected carriers linked to differing amplitudes of the parasitic hole current flowing from GaAs to Co-Fe-B in both cases.

DOI: 10.1103/PhysRevApplied.8.054027

I. INTRODUCTION

The use of the electron spin instead of its charge to design electronic devices with alternative functionalities [1] has stimulated intense investigation of spin properties in hybrid ferromagnetic-semiconductor systems in the past decade [2–10]. In spin light-emitting diodes (spin LEDs) based on a quantum well (QW), the circular polarization of the emitted electroluminescence reflects the electron spin polarization injected in the conduction band of the device due to optical selection rules [11]. This link allows us to quantify the efficiency of the spin injection. For future applications, these spin LEDs present the ability to transfer the electron spin information into the photon helicity and could be used in potential optical telecommunication devices [12–14].

Among all of the methods proposed to date to generate spin-polarized currents in semiconductors, an efficient solution at room temperature consists of injecting spin-polarized electrons from a ferromagnetic injector through a tunnel barrier (e.g., an oxide tunnel barrier like MgO [6,15–21]), in order to overcome the problem of conductivity mismatch between the metal and the semiconductor [22]. Thus far, in-plane CoFe/MgO [6] and in- and out-of-plane Co-Fe-B/MgO [16–21] injectors have exhibited the highest spin-injection yield into (Al,Ga)As, at both low temperature and room temperature under a perpendicular magnetic field at saturation. The electroluminescence polarization can reach values of up to 50% at 100 K and 32% at 300 K for CoFe/MgO in-plane injectors [6] and 37%–42% at 25 K at saturation for Co-Fe-B/MgO in-plane spin injectors [16,17]. This large polarization could result from spin-filtering effects linked to the nonequivalent attenuation of the evanescent wave functions inside the MgO barrier depending on their symmetries [23].

For practical applications, the influence of the bias and the current on the electrical spin-injection efficiency in such devices has to be understood. To date, it has been investigated in different types of hybrid ferromagnet-semiconductor systems: unipolar devices studied with the Kerr rotation technique [24], nonlocal four-terminal full-electrical devices and three-terminal full-electrical [25,26] or bipolar devices such as spin LEDs [6,7,27–31]. Among these studies, several investigations have been performed on spin LEDs based on Schottky [7,28,29,31], Al_2O_3 [27,30], or MgO barriers [6]. For the final option, a detailed understanding of the dependence of the

*yuan.lu@univ-lorraine.fr
†renucci@insa-toulouse.fr

spin-injection efficiency as a function of the bias is sill lacking. This dependence may depend on the metal-oxide-semiconductor interface, which has been explored in different systems in view of spin injection and detection [32–36]. In this paper, we investigate the influence of the MgO tunnel-barrier growth process on the current and bias dependence of the electrical spin injection into an (In, Ga)As/GaAs quantum-well light-emitting diode. The properties of the Co-Fe-B/MgO/GaAs interfaces are engineered thanks to the use of two types of growth for the textured MgO tunnel barriers, which are fabricated either by sputtering or by molecular beam epitaxy (MBE).

II. SAMPLES AND EXPERIMENTAL METHODS

The schematics of the spin-LED structure is displayed in Fig. 1(a). The *p-i-n* LED device grown by MBE contains a single 10-nm $In_{0.1}Ga_{0.9}As$/GaAs quantum well in the intrinsic region. The full sequence of the semiconductor structure is as follows: *p*-GaAs:Zn(001) substrate ($p = 2\times10^{19}$ cm^{-3})/500-nm *p*-GaAs:Be ($p=2\times10^{19}$ cm^{-3})/200-nm *p*-GaAs:Be ($p=2\times10^{18}$ cm^{-3})/50-nm undoped GaAs/10-nm undoped $In_{0.1}Ga_{0.9}As$/50-nm undoped GaAs/50-nm *n*-GaAs:Si ($n = 10^{16}$ cm^{-3}). The LEDs are passivated with arsenic in the semiconductor MBE chamber and then transferred through air into a second MBE-sputtering interconnected system.

The As capping layer is first desorbed at 300 °C in the MBE chamber. Two methods are then used to grow the MgO layer. Either the MgO layer is grown by MBE at 250 °C after As desorption or we transfer the sample through ultrahigh vacuum to a sputtering chamber to grow the MgO layer (in the latter case, a target of MgO is directly used for sputtering in Ar gas with a pressure of 10^{-2} mbar). In both cases [see Fig. 1(b)], the MgO layer has the same thickness of 2.5 nm, measured by transmission electron microscopy (TEM). Finally, the 3-nm $Co_{0.4}Fe_{0.4}B_{0.2}$ spin injector and 5-nm Ta protection layer are deposited by sputtering in both cases. Hereafter, we use the terms MBE and sputtering sample to refer to different spin LEDs with MgO prepared by the two different methods. Concerning device fabrication, 300-μm-diameter circular mesas are then processed using standard UV photolithography and etching techniques. Finally, the processed wafers are cut into small pieces to perform rapid temperature annealing at different temperatures for 3 min.

For the polarization-resolved electroluminescence (EL) measurements, the spin LED is placed into a Helmholtz-split magnetic coil providing a maximum magnetic field (B) of 0.8 T normal to the sample plane. The sample is excited with squared pulses at 50 kHz (a pulse width of 1 μs) in order to avoid the Joule effect. The EL signal is detected in the Faraday geometry. The EL circular-polarization degree P_c is analyzed through a $\lambda/4$ wave plate and a linear analyzer. P_c is defined as $P_c = (I^+ - I^-)/(I^+ + I^-)$, where I^+ and I^- are the intensities of the right and left circularly polarized components of the luminescence, respectively. The electroluminescence circular polarization P_c associated with the E_1-HH_1 exciton QW (XH) transition corresponds to the electron spin-polarization degree.

III. RESULTS AND DISCUSSION

A. Electroluminescence circular polarization

Figure 1(c) shows a typical cw EL spectra for a sputtering spin LED (annealed at 300 °C) acquired under a bias of $V = 2.4$ V for $B = 0.8$ T at 25 K. We check to see that the magnetic circular dichroism is less than 1% at 0.8 T [20,37]. The EL polarization reaches $P_c = 21.0 \pm 1.5\%$ for $B = 0.8$ T at 25 K, and it is still about $P_c = 20.0 \pm 1.5\%$ at 250 K (not shown). As expected from optical selection rules [11], the measured EL circular polarization detected along the growth axis increases with the applied longitudinal magnetic field [Fig. 1(d)] due to the progressive increase of the projection of the magnetization along the growth axis.

Note that the maximal applied magnetic field of 0.8 T is not enough to saturate the magnetization along the growth axis. In order to extrapolate P_c at saturation, we multiply P_c (0.8 T) by a factor $M_{\text{saturation}}/M(0.8\ T) \sim 1.75$ based on the results obtained with a superconducting quantum-interference device on this sample in Ref. [17]. This extrapolation leads to a rough estimation of P_c at a saturation of about $37.0 \pm 1.5\%$ at 25 K and $35.0 \pm 1.5\%$ at 250 K. Taking into account the spin relaxation during the electron lifetime in the quantum well, by measuring the electron spin lifetime τ_s and the electron

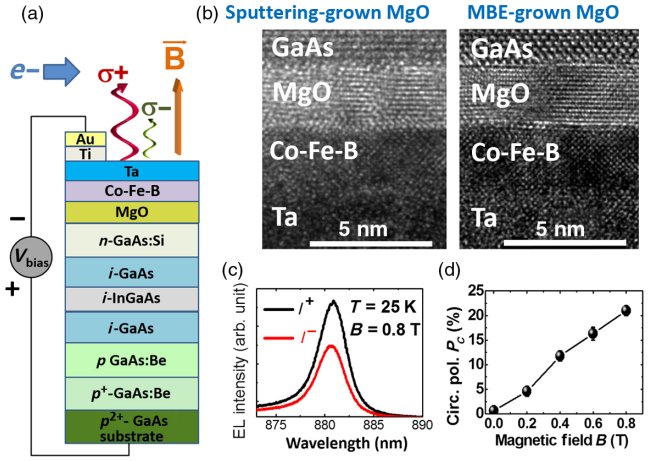

FIG. 1. (a) Schematics of the spin-LED structure with a single (In, Ga)As/GaAs quantum well. (b) TEM cross section of Co-Fe-B/MgO/GaAs interfaces for (left panel) a sputtering sample and (right panel) a MBE sample. (c) Polarized electroluminescence spectra (I^+ and I^-) for the sputtering sample ($T_{\text{an}} = 300$ °C) at $T = 25$ K for $B = 0.8$ T. (d) EL circular polarization as a function of the applied longitudinal magnetic field for the same sample used in (c).

lifetime τ at 25 K [17], one can estimate an injected spin polarization $P_e \sim 51\%$ at 25 K [$P_e = P_c/F$, with $F = 1/(1+\tau/\tau_s) \sim 0.72$]. This value proves the efficiency and robustness of the spin-injection process into an (In, Ga)As/GaAs QW [4,31,38] with Co-Fe-B/MgO electrodes [20].

B. Bias dependence of the electroluminescence circular polarization

Figure 2(a) shows the variation of P_c as a function of the current injected in the spin LEDs annealed at 300 °C for the sputtering and MBE samples. It appears clearly that P_c is rather stable (just slightly decreasing) in the former case, whereas P_c decreases abruptly when the current increases in the latter case. We observe that this trend does not depend on the annealing temperature T_{an} in the range 200 °C–350 °C [the inset of Fig. 2(a) shows, for example, very similar dependences of P_c as a function of current for sputtering samples annealed at 200 °C, 270 °C, and 300 °C].

We also measure P_c as a function of V_{bias} applied to the spin LEDs [Fig. 2(b)], which reveals the same trend as the current dependence. Concerning the dependence of the circular polarization of EL as a function of V_{bias}, several investigations have been performed previously on spin LEDs based on Schottky barriers [7,28,29] or oxide barriers [6,27,30].

For a thin Schottky barrier based on a highly *n*-doped semiconductor layer at the interface, it has been demonstrated that a very significant part of the bias drops on the semiconductor emitting zone—even in the regime of photon emission. In this case, the dependence of the electroluminescence circular polarization on bias is usually explained by the complex bias dependence of the ratio τ/τ_s between the electron lifetime τ and the electron spin-relaxation time τ_s in the emitting zone [7,29].

For oxide tunnel barriers, the applied bias drops on the *p-i-n* part of the device during a first step. Once enough holes are accumulated at the oxide-semiconductor interface [30] [see Fig. 5(b)], the bias drops also on the oxide barrier, allowing the bending of the tunnel barrier and the alignment of the semiconductor conduction band on the ferromagnetic-metal Fermi level. Then electrons start to be efficiently injected from the ferromagnetic to the semiconductor system and electroluminescence appears: we have confirmed this general trend for our device using the self-consistent Poisson-Schrödinger code from Ref. [39] (see Fig. 4). The carriers are injected with increasing kinetic energy for increasing biases. Thus, these electrons can encounter a spin relaxation due to the Dyakonov-Perel mechanism [40], leading to the decreasing behavior of the electroluminescence circular polarization as a function of the applied voltage [6,27,30].

From a general point of view, the electroluminescence circular-polarization rate detected in the quantum well can

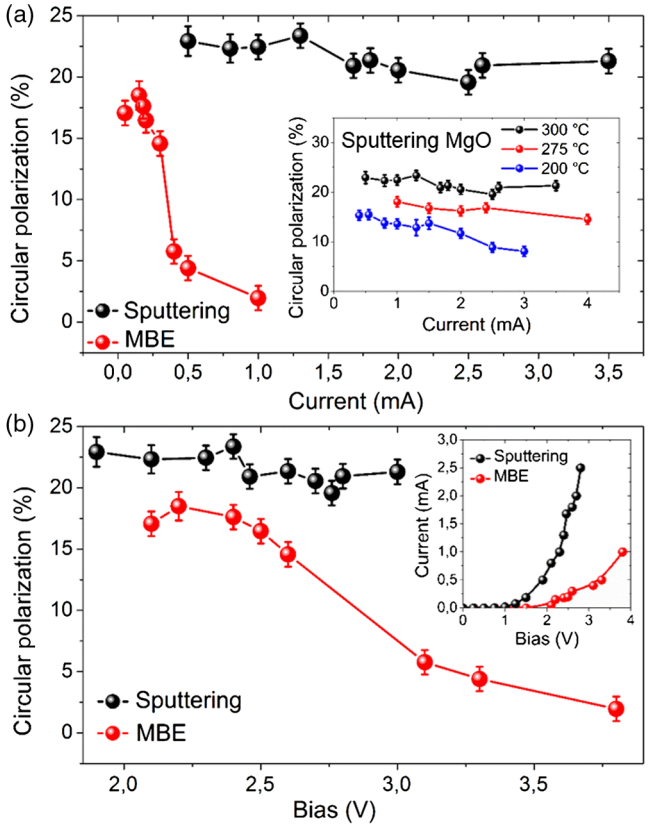

FIG. 2. (a) EL circular polarization as a function of the current for sputtering and MBE samples annealed at 300 °C. (Inset) EL circular polarization as a function of the current for the sputtering sample for different annealing temperature T_{an}. (b) EL circular polarization as a function of the applied bias. (Inset) I-V_{bias} curves for both samples. $T = 25$ K, $B = 0.8$ T.

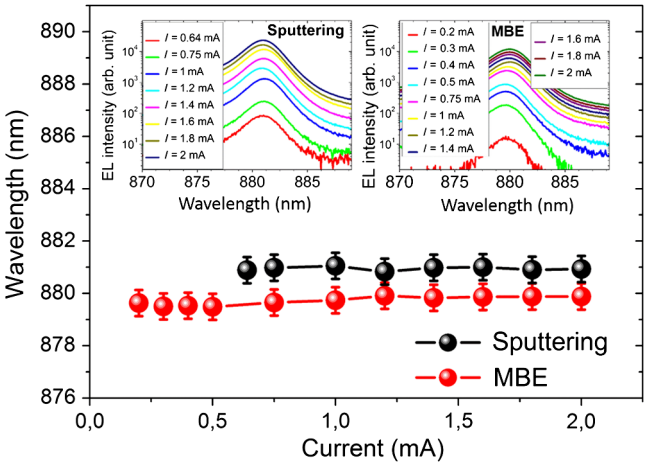

FIG. 3. Spin LEDs annealed at 300 °C. Central wavelength of the EL emission as a function of the injected current for a sputtering sample (the black spheres) and a MBE sample (the red spheres). The spectral resolution is 1 nm. (Top-left inset) EL spectra as a function of current for the sputtering sample. (Top-right inset) EL spectra as a function of current for the MBE sample.

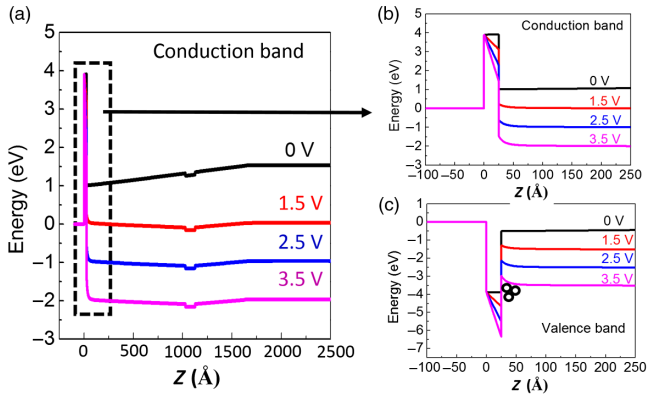

FIG. 4. Band structure calculations using a one-dimensional Poisson-Schrödinger solver [39] at 25 K. (a) Conduction band as a function of z (the growth axis) under applied bias. (b) The same physical quantity with an enlargement of the first 250 Å. (c) Valence band as a function of z under applied bias with an enlargement of the first 250 Å. The open circles represent the hole accumulation.

be written as $P_c = P_0\ (E_k)/(1 + \tau/\tau_s)$. τ and τ_s are the electron lifetime and the electron spin-relaxation time in the (In, Ga)As/GaAs QW, respectively. $P_0\ (E_k)$ is the electron spin polarization just beneath the MgO/GaAs interface when the electrons have been injected with a kinetic energy E_k and have thermalized in the bottom of the conduction band. As shown in Fig. 2(b), P_c clearly decreases faster for MBE spin LEDs when increasing V_{bias}. The fact that we observe no Stark shift on the XH transition of the quantum well (see Fig. 3) for the two types of samples indicates that the applied bias does not drop in the intrinsic region of the *p-i-n* junction once the bias threshold required to get electroluminescence is reached. One can thus consider that the variation of the ratio τ/τ_s due to a variation of electric field on the QW is not responsible for the observed decays of P_c as a function of bias or current.

C. Evidence of the parasitic hole current tunneling through MgO barriers

The overall differing qualitative behavior of the decrease of P_c as a function of bias (or current) in the two different samples (MBE and sputtering) could originate from a nonequivalent balance of the biases that drop, respectively, on the tunnel barrier and on the semiconductor part of the devices. This point is linked to the existence of a weak or large hole parasitic current flowing through the MgO tunnel barrier. Indeed, as explained in Ref. [30] for spin LEDs based on oxide tunnel barriers, the total current flowing in the device contains a parasitic current due to electrons that cross the tunnel barrier from the metal to the valence band of the semiconductor. It can be seen equivalently as a hole current flowing from the GaAs valence band to Co-Fe-B through MgO [see Fig. 5(b)]. This parasitic channel can be considered a shunt resistor in parallel to the tunnel barrier.

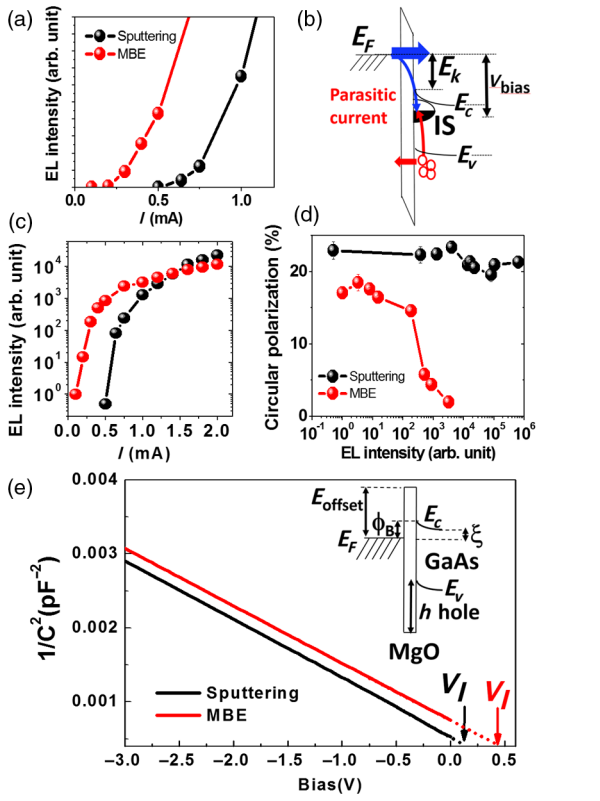

FIG. 5. (a) EL intensity as a function of the current for a sputtering sample (the black spheres) and a MBE sample (the red spheres) in the low current regime (≤1 mA). (b) Scheme of spin injection with parasitic current; see the text. (c) EL intensity (log scale) as a function of the current for the sputtering sample (the black spheres) and the MBE sample (the red spheres). (d) Figure of merit: EL circular polarization versus EL intensity for the sputtering sample (the black spheres) and the MBE sample (the red spheres). (e) $1/C^2$ curves as a function of V extracted from the high-frequency (1 MHz) CV curves measured at room temperature for Au/MgO(2.5 nm)/n-GaAs(001) samples annealed at 300 °C (the contact diameter is 300 μm), where the MgO layers are deposited either by sputtering (the black line) or by MBE (the red line). The vertical arrows indicate the intercept voltage V_I for the sputtering (black) and MBE (red) samples. (Inset) Band scheme at the Co-Fe-B/MgO/GaAs interface; see the text. The spin LEDs are annealed at 300 °C. $T = 25$ K.

In this picture, this current is smaller for the MBE sample. Because of this weak shunt, the voltage drop on the tunnel barrier is large. In principle, a reduced leakage current induces a smaller threshold current to get the electroluminescence [30]. We do indeed observe this effect. Figure 5(a) shows the EL intensity as a function of the current through the device for both kinds of samples. We observe that the EL threshold is smaller for the MBE spin LED. As the voltage drop on the tunnel barrier is larger for this sample, the initial kinetic energy E_k is larger for a given bias voltage compared to the sputtering samples. As in bulk III–V semiconductors, the Dyakonov-Perel spin-relaxation-process efficiency increases with E_k [31,40], and it leads to a polarization

P_0 (E_k) strongly decreasing when the applied bias increases for the MBE sample. This trend could explain the observed clear decay of EL circular polarization as a function of the applied bias or current (Fig. 2) [41].

For the sputtering samples, the leakage parasitic current is stronger, as is the shunt effect (the measured EL threshold is larger than the one for the MBE sample), so the voltage drop on the tunnel barrier is smaller for a given total applied voltage V_{bias}. The efficiency of the Dyakonov-Perel mechanism is thus weaker, and it leads to a P_0 (E_k) slightly decreasing when the applied bias increases [Fig. 2(b)]. Note that the comparison of $I(V_{bias})$ characteristics for the two samples indicates that the current is larger in the sputtering sample [see the inset in Fig. 2(b)] for the range of biases explored. A significant part of the current may be caused by the parasitic leakage tunnel current through the MgO barrier.

D. Comparison of MgO barrier height for holes in the two types of tunnel barriers

A larger parasitic hole tunnel current for sputtering samples can have different origins. First, part of this current could be due to the presence of localized interface states and/or defect states (IS) at the MgO/GaAs interface [27] [see Fig. 5(b)]. The density of these states could differ between the full MBE-grown GaAs/MgO interface and the one obtained by a mixed growth method (MBE and sputtering) where a chamber transfer occurs. Second, part of the parasitic current could also be due to a direct tunneling of holes [27,30] through MgO [see Fig. 5(b)] and would thus depend on the height of the MgO tunnel barrier seen by the holes, which could be varied with the MgO growth process.

In order to go further in the understanding of the interface, we study the room-temperature electrical properties of a Au/MgO(2.5 nm)/n-doped ($n = 5 \times 10^{16}$ cm^{-3}) GaAs(001) structure annealed at 300 °C using CV methods. The MgO barriers have been prepared either by MBE or by sputtering methods, as those of the spin LED. Practical details about the CV experiments can be found in Ref. [43].

First, the analysis of CV measurements proves, for both kinds of samples, the existence of interface states (extracted using Terman's method [44]) in the upper-half part of the band gap with a density of states (DOS) larger than about 3×10^{17} states/eV m^2. However, as the DOSs are quite similar for both kinds of samples, the presence of these states, if taken alone, cannot explain the difference in the EL thresholds. Let us now examine the height h_{hole} of the hole tunnel barriers for each sample [see the inset in Fig. 5(e)]. This height h_{hole} can be expressed as $h_{hole} = E_{gap}^{MgO} - (E_{gap}^{GaAs} - \phi_B) - E_{offset}$, where E_{gap}^{MgO} and E_{gap}^{GaAs} are the band gaps of MgO and GaAs, respectively, and E_{offset} is the band offset between the Co-Fe-B Fermi level and the bottom of the conduction band of MgO at the Co-Fe-B/MgO interface; ϕ_B is defined by the energy difference between the position of the bottom of the conduction band of GaAs at the MgO/GaAs interface and the Fermi level at zero bias.

Figure 5(e) shows the $1/C^2$ curves extracted from the high-frequency (1 MHz) CV curves measured at room temperature with MgO layers deposited either by MBE or by sputtering. Under reverse-bias voltages, the linear dependence of the $1/C^2$ versus bias voltage shows that the metal-oxide-semiconductor structures operate under depletion or deep-depletion mode. The barrier heights are calculated from the $1/C^2$ versus bias voltage under reverse-bias voltage using the following relation, $\phi_B = eV_I + k_BT + \xi$, where V_I is the voltage intercept of the extrapolated $1/C^2$ curve with the voltage axis, e is the elementary charge, and k_B is the Boltzmann constant. $\xi = k_BT\ln(N_c/N_d)$ is the difference between the energies of the bottom of conduction band and the Fermi level in bulk GaAs ($\xi = 56$ meV). Here, N_d is the donor concentration and $N_c = 2/h^3(2\pi m^* k_BT)^{3/2}$ is the effective density of states, where h is Planck's constant and m^* is the effective mass for conduction electrons in the zone center. We find that ϕ_B is larger for a MBE sample (1.00 eV) than for a sputtering sample (0.73 eV). These distinct values confirm that MgO/GaAs interfaces are clearly different from one growth technique to another.

If one assumes a comparable band offset E_{offset} for the two types of samples, a weaker value for ϕ_B for sputtering samples (0.73 instead of 1.00 eV for MBE samples) directly leads to a smaller tunnel-barrier height h_{hole} for the holes, which would explain the existence of a larger parasitic hole current for these sputtering samples. (Moreover, previous studies have demonstrated that the band offset E_{offset} can also depend on the MgO growth technique [45].) Hence, we conclude that the difference of hole tunnel-barrier height is more likely responsible for the difference in the EL threshold between samples grown by MBE and by sputtering.

E. Electroluminescence circular polarization and intensity

As electrons are injected with a lower kinetic energy for the sputtering sample, their capture by the quantum well is more efficient [46] than in the case of the MBE sample. This finding could explain that, at higher currents [>1.5 mA; see Fig. 5(c)], the intensity of EL of the sputtering sample surpasses that of the MBE sample. Finally, we plot the figure of merit of P_c versus the EL intensity in Fig. 5(d). It appears to be clear that the compromise between high P_c and high EL intensity (for comparable electrical power consumption of the two samples, e.g., 2.3 mW for the sputtering sample instead of 3.8 mW for the MBE sample at $I = 1$ mA) is strongly dependent on the MgO growth process. Note that all of the trends reported for our samples with $T_{an} = 300$°C are also observed for samples with $T_{an} = 350$ °C (not shown).

IV. CONCLUSION

In this paper, we investigate the influence of the MgO/GaAs interface on the current and bias dependence of the electrical spin injection into an (In, Ga)As/GaAs quantum-well light-emitting diode using textured MgO tunnel barriers fabricated either by sputtering or by MBE. An original point of this work is to use the complementary technique of capacitance-voltage measurements in addition to electroluminescence to get a deeper understanding of the metal/MgO/GaAs interface. We attribute the different behaviors observed on the two types of samples to the different kinetic energies of the injected carriers that result from the different Co-Fe-B/MgO/GaAs interfaces.

In view of future applications, our results show that the compromise between high electroluminescence circular polarization and high electroluminescence intensity can be modified by changing the MgO growth process. Here we reported on how the bias dependence of spin injection can be engineered thanks to different growth techniques of the MgO/GaAs interface. Finally, the understanding of the dependence of the spin-injection efficiency as a function of the applied bias would strongly benefit from the study of a three-terminal device [47] in order to apply or measure independently the voltage drops on the tunnel barrier and on the semiconductor part of the device [48].

ACKNOWLEDGMENTS

This work was supported by the joint French National Research Agency (ANR)–National Natural Science Foundation of China (NSFC) SISTER project (Grants No. ANR-11-IS10-0001 and No. NNSFC 61161130527) and ENSEMBLE projects (Grants No. ANR-14-0028-01 and No. NNSFC 61411136001), by the French ANR research project INSPIRE (ANR-10-BLAN-1014), and by NEXT Grant No. ANR-10-LABX-0037 in the framework of the Programme des Investissements d'Avenir. Experiments were performed using equipment from the platform TUBE-Davm funded by FEDER (EU), ANR, the Region Lorraine, and Grand Nancy.

[1] S. Datta and B. Das, Electronic analog of the electro-optic modulator, Appl. Phys. Lett. **56**, 665 (1990).

[2] R. Fiederling, M. Keim, G. Reuscher, W. Ossau, G. Schmidt, A. Waag, and L. W. Molenkamp, Injection and detection of a spin-polarized current in a light-emitting diode, Nature (London) **402**, 787 (1999).

[3] Y. Ohno, D. K. Young, B. Beschoten, F. Matsukura, H. Ohno, and D. D. Awschalom, Electrical spin injection in a ferromagnetic semiconductor heterostructure, Nature (London) **402**, 790 (1999).

[4] H. J. Zhu, M. Ramsteiner, H. Kostial, M. Wassermeier, H. P. Schnherr, and K. H. Ploog, Room-Temperature Spin Injection from Fe into GaAs, Phys. Rev. Lett. **87**, 016601 (2001).

[5] A. Hanbicki, O. M. J. van 't Erve, R. Magno, G. Kioseoglou, C. H. Li, and B. T. Jonker, Analysis of the transport process providing spin injection through an Fe/Al-Ga-As Schottky barrier, Appl. Phys. Lett. **82**, 4092 (2003).

[6] X. Jiang, R. Wang, R. M. Shelby, R. M. Macfarlane, S. R. Bank, J. S. Harris, and S. S. P. Parkin, Highly Spin-Polarized Room-Temperature Tunnel Injector for Semiconductor Spintronics Using MgO(100), Phys. Rev. Lett. **94**, 056601 (2005).

[7] C. Adelmann, X. Lou, J. Strand, C. J. Palmstrom, and P. A. Crowell, Spin injection and relaxation in ferromagnet-semiconductor heterostructures, Phys. Rev. B **71**, 121301(R) (2005).

[8] M. Holub, J. Shin, D. Saha, and P. Bhattacharya, Electrical Spin Injection and Threshold Reduction in a Semiconductor Laser, Phys. Rev. Lett. **98**, 146603 (2007).

[9] I. Zutic, J. Fabian, and S. D. Sarma, Spintronics: Fundamentals and applications, Rev. Mod. Phys. **76**, 323 (2004).

[10] S. P. Dash, S. Sharma, R. S. Patel, M. P. de Jong, and R. Jansen, Electrical creation of spin polarization in silicon at room temperature, Nature (London) **462**, 491 (2009).

[11] M. Dyakonov, *Spin Physics in Semiconductors*, Springer Series in Solid-State Sciences Vol. 157 (Springer-Verlag, Berlin, 2008).

[12] N. Nishizawa, K. Nishibayashi, and H. Munekata, A spin light emitting diode incorporating ability of electrical helicity switching, Appl. Phys. Lett. **104**, 111102 (2014).

[13] N. Nishizawa, K. Nishibayashi, and H. Munekata, Pure circular polarization electroluminescence at room temperature with spin-polarized light-emitting diodes, Proc. Natl. Acad. Sci. U.S.A. **114**, 1783 (2017).

[14] A. Joly, J. Frougier, G. Baili, M. Alouini, J. M. George, I. Sagnes, and D. Dolfi, Theoretical and experimental investigation of optically spin-injected VECSEL, Proc. SPIE Int. Soc. Opt. Eng. **9755**, 97551E (2016).

[15] T. Manago, A. Sinsarp, and H. Akinaga, Growth condition dependence of spin-polarized electroluminescence in Fe/MgO/light-emitting diodes, J. Appl. Phys. **102**, 083914 (2007).

[16] Y. Lu, V. G. Truong, P. Renucci, M. Tran, H. Jaffrès, C. Deranlot, J. M. George, A. Lematre, Y. Zheng, D. Demaille, P. H. Binh, T. Amand, and X. Marie, MgO thickness dependence of spin injection efficiency in spin-light emitting diodes, Appl. Phys. Lett. **93**, 152102 (2008).

[17] P. Barate, S. Liang, T. T. Zhang, J. Frougier, M. Vidal, P. Renucci, X. Devaux, B. Xu, H. Jaffres, J. M. George, X. Marie, M. Hehn, S. Mangin, Y. Zheng, T. Amand, B. Tao, X. F. Han, Z. Wang, and Y. Lu, Electrical spin injection into In-Ga-As/GaAs quantum wells: A comparison between MgO tunnel barriers grown by sputtering and molecular beam epitaxy methods, Appl. Phys. Lett. **105**, 012404 (2014).

[18] P. Renucci, V. G. Truong, H. Jaffrès, L. Lombez, P. H. Binh, T. Amand, J. M. George, and X. Marie, Spin-polarized electroluminescence and spin-dependent photocurrent in

hybrid semiconductor/ferromagnetic heterostructures: An asymmetric problem, Phys. Rev. B **82**, 195317 (2010).

[19] V. G. Truong, P. H. Binh, P. Renucci, M. Tran, Y. Lu, H. Jaffrès, J. M. George, C. Deranlot, A. Lemaitre, T. Amand, and X. Marie, High speed pulsed electrical spin injection in spin-light emitting diode, Appl. Phys. Lett. **94**, 141109 (2009).

[20] S. H. Liang *et al.*, Large and robust electrical spin injection into GaAs at zero magnetic field using an ultrathin Co-Fe-B/MgO injector, Phys. Rev. B **90**, 085310 (2014).

[21] B. S. Tao, P. Barate, J. Frougier, P. Renucci, B. Xu, A. Djeffal, H. Jaffrès, J. M. George, X. Marie, S. Petit-Watelot, S. Manging, X. F. Han, Z. G. Wang, and Y. Lu, Electrical spin injection into GaAs based light emitting diodes using perpendicular magnetic tunnel junction-type spin injector, Appl. Phys. Lett. **108**, 152404 (2016).

[22] A. Fert and H. Jaffrès, Conditions for efficient spin injection from a ferromagnetic metal into a semiconductor, Phys. Rev. B **64**, 184420 (2001).

[23] W. H. Butler, X. G. Zhang, T. C. Schulthess, and J. M. MacLaren, Spin-dependent tunneling conductance of Fe/MgO/Fe sandwiches, Phys. Rev. B **63**, 054416 (2001).

[24] S. A. Crooker, M. Furis, X. Lou, C. Adelmann, D. L. Smith, C. J. Palmstrom, and P. A. Crowell, Imaging spin transport in lateral ferromagnet/semiconductor structures, Science **309**, 2191 (2005).

[25] X. Lou, C. Adelmann, S. A. Crooker, E. S. Garli, J. Zhang, K. S. Madhukar Reddy, S. D. Flexner, C. J. Palmstrom, and P. A. Crowell, Electrical detection of spin transport in lateral ferromagnet-semiconductor devices, Nat. Phys. **3**, 197 (2007).

[26] M. Tran, H. Jaffrès, C. Deranlot, J. M. George, A. Fert, A. Miard, and A. Lematre, Enhancement of the Spin Accumulation at the Interface between a Spin-Polarized Tunnel Function and a Semiconductor, Phys. Rev. Lett. **102**, 036601 (2009).

[27] V. F. Motsnyi, P. Van Dorpe, W. V. Roy, E Goovaerts, V. I. Safarov, G. Borghs, and J. De Boeck, Optical investigation of electrical spin injection into semiconductors, Phys. Rev. B **68**, 245319 (2003).

[28] X. Y. Dong, C. Adelmann, J. Q. Xie, C. J. Palmstrom, X. Lou, J. Strand, P. A. Crowell, J. P. Barnes, and A. K. Petford-Long, Spin injection from the Heusler alloy Co_2 MnGe into $Al_{0.1}Ga_{0.9}$ As-Ga-As heterostructures, Appl. Phys. Lett. **86**, 102107 (2005).

[29] C. Adelmann, J. L. Hilton, B. D. Schultz, S. McKernan, C. J. Palmstrom, X. Lou, H. S. Chiang, and P. A. Crowell, Spin injection from perpendicular magnetized ferromagnetic δ-MnGa into (Al,Ga)As heterostructures, Appl. Phys. Lett. **89**, 112511 (2006).

[30] W. Van Roy, P. Van Dorpe, J. De Boeck, and G. Borghs, Spin injection in LEDs and in unipolar devices, J. Mater. Sci. Eng. B **126**, 155 (2006).

[31] M. C. Hickey, S. N. Holmes, T. Meng, I. Farrer, G. A. C. Jones, D. A. Ritchie, and M. Pepper, Strongly bias-dependent spin injection from Fe into *n*-type GaAs, Phys. Rev. B **75**, 193204 (2007).

[32] F. Rortais, C. Vergnaud, C. Ducruet, C. Beign, A. Marty, J. P. Attane, J. Widiez, H. Jaffres, J. M. George, and M. Jamet, Electrical spin injection in silicon and the role of defects, Phys. Rev. B **94**, 174426 (2016).

[33] R. Ohsugi, Y. Kunihashiz, H. Sanada, M. Kohda, H. Gotoh, T. Sogawa, and J. Nitta, Bias dependence of spin injection/transport properties of a perpendicularly magnetized FePt/MgO/GaAs structure, Appl. Phys. Express **9**, 043002 (2016).

[34] S. Lee, N. Yamashita, Y. Ando, S. Miwa, Y. Suzuki, H. Koike, and M. Shiraishi, Investigation of spin scattering mechanism in silicon channels of Fe/MgO/Si lateral spin valves, Appl. Phys. Lett. **110**, 192401 (2017).

[35] R. Roca, N. Nishizawa, K. Nishibayashi, and H. Munekata, Investigation of helicity-dependent photocurrent at room temperature from a Fe/x-AlO_x/*p*-GaAs Schottky junction with oblique surface illumination, Jpn. J. Appl. Phys. **56**, 04CN05 (2017).

[36] S. Sharma, A. Spiesser, S. P. Dash, S. Iba, S. Watanabe, B. J. van Wees, H. Saito, S. Yuasa, and R. Jansen, Anomalous scaling of spin accumulation in ferromagnetic tunnel devices with silicon and germanium, Phys. Rev. B **89**, 075301 (2014).

[37] C. Rinaldi, M. Cantoni, M. Marangoni, C. Manzoni, G. Cerullo, and R. Bertacco, Wide-range optical spin orientation in Ge from near-infrared to visible light, Phys. Rev. B **90**, 161304(R) (2014).

[38] C. H. Li, G. Kioseoglou, A. Petrou, M. Korkusinski, P. Hawrylak, and B. T. Jonker, Highly polarized emission from electrical spin injection into an InGaAs quantum well with free carriers, Appl. Phys. Lett. **103**, 212403 (2013).

[39] I. H. Tan, G. L. Snider, L. D. Chang, and E. L. Hu, A self-consistent solution of Schrödinger-Poisson equations using a nonuniform mesh, J. Appl. Phys. **68**, 4071 (1990).

[40] M. I. Dyakonov and V. I. Perel, Spin orientation of electrons associated with the interband absorption of light in semiconductors, J. Exp. Theor. Phys. **33**, 1053 (1971).

[41] Note that we can roughly estimate, for our MgO/GaAs barriers and from an effective mass two-band model [42], the characteristic energy window of carrier tunnel injection at about 300 meV below the Fermi level. Note that this window is pretty low compared to the typical energy scale of the density of state, and it should not induce a significant loss of the spin polarization.

[42] J. C. Slonczewski, Conductance and exchange coupling of two ferromagnets separated by a tunneling barrier, Phys. Rev. B **39**, 6995 (1989).

[43] J. C. LeBreton, S. LeGall, G. Jezequel, B. Lepine, P. Schieffer, and P. Turban, Transport property study of MgO-GaAs(001) contacts for spin injection devices, Appl. Phys. Lett. **91**, 172112 (2007).

[44] L. M. Terman, An investigation of surface states at a silicon/silicon oxide interface employing metal-oxide-silicon diodes, Solid State Electron. **5**, 285 (1962).

[45] For example, a larger E_{offset} (of approximately 0.5 eV) was observed by P. G. Mather, J. C. Read, and R. A. Buhrman, Disorder, defects, and band gaps in ultrathin (001)MgO tunnel barrier layers, Phys. Rev. B **73**, 205412 (2006)] for sputtering MgO than for electron-beam-evaporated MgO in Fe/MgO/Fe structures. This difference would also induce a smaller h_{hole} for sputtering samples.

[46] D. Y. Oberli, J. Shah, J. L. Jewell, and T. C. Damen, Dynamics of carrier capture in an InGaAs/GaAs quantum well trap, Appl. Phys. Lett. **54**, 1028 (1989).

[47] E. Johnston-Halperin, D. Lofgreen, R. K. Kawakami, D. K. Young, L. Coldren, A. C. Gossard, and D. D. Awschalom, Spin-polarized Zener tunneling in (Ga,Mn)As, Phys. Rev. B **65**, 041306 (2002).

[48] Note that taking an Ohmic contact at the MgO/GaAs interface requires a strong *n* doping of GaAs at the interface. This strong doping would clearly modify the device from the point of view of its band scheme, and it could lead to a nonoptimal device from the point of view of the spin transport itself.